Fast 3-D Electrical Impedance Spectroscopic Imaging Using Extended Joint Sparsity

Fast 3-D Electrical Impedance Spectroscopic Imaging Using Extended Joint Sparsity

Yunjie Yang* and Jiabin Jia

Agile Tomography Group, School of Engineering, The University of Edinburgh, Edinburgh, UK

*Email: y.yang@ed.ac.uk

ABSTRACT

The problem of efficient, high-resolution 3-D image reconstruction from multi-frequency Electrical Impedance Tomography (EIT) data sequences has attracted significant attention from researchers due to its practical importance in process analysis of chemical or biomedical engineering. To tackle this challenge, we propose in this paper a novel image reconstruction algorithm exploiting the spatial-frequency correlations of the image series, in order to perform efficient 3-D image reconstructions using multi-frequency EIT data. The main contribution of this paper includes the development of an extended joint sparsity framework. This combines the structural characters of time-difference conductivity distribution and the structural correlations among frequency-difference images. In addition, a dynamic 3-D structural feature extraction method was developed to iteratively group the voxels with similarities. The Alternating Direction Method of Multipliers framework was employed to solve the inversion problem. Phantom experiments were conducted to verify the performance of this new method. The results suggest that the algorithm proposed is fast, stable and yields superior reconstructions when compared with other state-of-the-art algorithms.

Keywords multi-frequency electrical impedance tomography, joint sparsity, 3-D image reconstruction

Industrial Application (Recommended Sector or 'General'): General.

1 INTRODUCTION

Electrical Impedance Tomography (EIT) is a tomographic imaging modality, which can non-intrusively reveal conductivity distribution in either 2-D or 3-D sensing regions by injecting currents in such regions and measuring induced potentials on boundary electrodes (Malone et al., 2014). In view of its high-speed, non-radiation and non-intrusive sensing ability, EIT has been investigated extensively in industrial process imaging (Dong et al., 2006, Lee et al., 2014) and biomedical imaging (Yin et al., 2018) in recent decades. Compared with other tomography modalities, e.g. Computed Tomography (CT), the application scope of EIT has been boosted by its high temporal resolution, e.g. ~1000 frames per second (Wang et al., 2005), but limited by the low spatial resolution, e.g. ~10% of the sensor diameter (Metherall et al., 1996). As an extension of mono-frequency EIT, multi-frequency EIT (mfEIT) (Yang and Jia, 2017b) using spectroscopic current injection has emerged to acquire spectral electrical properties of sensing objects, which tends to be more attractive.

In mfEIT, the challenge of performing effective 3-D image reconstruction from multi-frequency data sequences has raised significant attention because of its practical importance in process analysis of chemical or biomedical engineering. In order to address this issue, in this work, we propose a novel image reconstruction algorithm by exploiting the spatial-frequency correlations of the image series, which enables simultaneous, high-performance 3-D impedance spectroscopic imaging using multi-frequency data. The key contribution of this paper lies in the development of an extended joint sparsity framework to combine the structural characters of time-difference (TD) conductivity variation and structural correlations among different frequency-difference (FD) images. Furthermore, a dynamic 3-D structural feature extraction method was developed to iteratively group the voxels demonstrating similar properties. The Alternating Direction Method of Multipliers (ADMM) framework was employed to solve the optimization problem. Phantom experiments were conducted to verify the performance of this new method. These results validate that the algorithm proposed is fast, stable and yields superior mfEIT reconstructions when compared with other state-of-the-art 3-D EIT image reconstruction algorithms, such as the one-step Gauss-Newton (GN) method with Laplacian regularizer (Yang et al., 2014).

2 FUNDAMENTAL OF MULTI-FREQUENCY EIT

EIT reconstructs images of conductivity inside the Region of Interest (ROI) based on transfer impedance measurements across a number of boundary electrodes (Yang and Jia, 2017a). The relationship between local conductivity and voltage distribution is governed by the following Complete Electrode Model (CEM) (Cheng et al., 1989, Somersalo et al., 1992) at the quasi-static limit

$$\begin{cases} \nabla \cdot \big(\sigma(x,y)\nabla u(x,y)\big) = 0, \ \ (x,y) \in \Omega \\ u + z_\ell \sigma \frac{\partial u}{\partial n} = U_\ell, \ (x,y) \in e_\ell, \ \ell = 1, \dots, \mathcal{g} \\ \int_{e_\ell} \sigma \frac{\partial u}{\partial n} dS = I_\ell \, , \ \ell = 1, \dots, \mathcal{g} \\ \sigma \frac{\partial u}{\partial n} = 0, \ (x,y) \in \partial\Omega \setminus \cup_{\ell=1}^{\mathcal{L}} e_\ell \end{cases} \tag{1}$$

where σ is the local conductivity in ROI, which is a 2-D or 3-D region $\Omega \subset \mathbb{R}^q \ (q = 2, 3)$, and u is the local electric potential; n is the outward unit norm of the boundary $\partial\Omega$; $\mathcal{g}$ denotes the number of sensing electrodes and e_ℓ represents the ℓ^{th} electrode; z_ℓ is the contact impedance of electrode e_ℓ; U_ℓ and I_ℓ denote respectively the electrical potential and current injected on e_ℓ.

Based on CEM, a linearized relation between conductivity variation and the induced changes in voltage measurements on boundary electrodes can be derived by assuming a local conductivity perturbation $\Delta\sigma \in \mathbb{R}^n$ in the ROI (Polydorides, 2009), which can be formulated as

$$\Delta V = J\Delta\sigma \tag{2}$$

where $\Delta V \in \mathbb{R}^m$, $J \in \mathbb{R}^{m\times n}$ represents respectively the boundary voltage changes induced by the conductivity perturbation and the Jacobian matrix indicating the sensitivity distribution of each measurement (Polydorides and Lionheart, 2002). Here, m denotes the number of measurements while n is number of pixels/voxels in the tomographic image.

As an emerging spectroscopic impedance imaging method, mfEIT applies multi-frequency current excitation to resolve frequency-dependent electrical properties of the imaging objects. In such context, Eq. (3) can be extended to comprise multi-frequency voltage measurements, which yields

$$K = JQ \tag{3}$$

where

$$K = [\Delta V_1, \quad \cdots \quad , \Delta V_p] \in \mathbb{R}^{m\times p} \tag{4}$$

$$Q = [\Delta\sigma_1, \quad \cdots \quad , \Delta\sigma_p] \in \mathbb{R}^{n\times p} \tag{5}$$

and K is the collection of p measurements; $\Delta V_i \in \mathbb{R}^m, (i = 1, \dots, p)$ is the measured voltage change vector induced by the i^{th} current frequency component; Q is a collection of p jointly spare solutions; $\Delta\sigma_i \in \mathbb{R}^n, (i = 1, \dots, p)$ represents the conductivity change vector demonstrated under the i^{th} current frequency setting. Under a 3-D sensing setup, a critical challenge is to efficiently and simultaneously estimate the conductivity under various frequency components, which represents a typical but large-scale inverse problem.

3 IMAGE RECONSTRUCTIN BASED ON EXTENDED JOINT SPARSITY

As an effective constraint, group sparsity has been investigated recently in solving EIT image reconstruction problem (Yang and Jia, 2017a). It extends the concept of sparsity by exploiting underlying structural information of conductivity distribution (Huang and Zhang, 2010). The former work using group sparsity in EIT image reconstruction generally deals with the structural characteristics of an individual image. Whilst in mfEIT image reconstruction, this problem has been extended with multiple measurement vectors and simultaneous reconstruction of images under all frequency components is

highly desirable.

In this work, an extended joint sparsity constrained image reconstruction algorithm is developed to fulfill this requirement. The basic idea is illustrated in Figure 1. A coarse mesh with 40 layers of voxels along the vertical direction is utilized in solving the inverse problem, where each layer is consisted of 812 voxels in the cylindrical area. For multi-frequency current excitations with frequencies ranging from f_0 to f_p, where f_0 is the basic frequency or reference frequency, the local structural information of an individual image at f_0 is firstly extracted by using TD imaging method (Yang and Jia, 2017b). The structural characteristics are represented by grouping voxels with similar conductivity variations. Compared with FD imaging, TD imaging can reveal more accurately the structural information due to its ability of eliminating the common errors from the sensor, model, etc. Next, the correlation of conductivity variation along frequencies are considered by grouping each row of the matrix $[\Delta\sigma_1, \cdots, \Delta\sigma_p]$ (see Figure 1, voxel *i* as an example), by considering the fact that the same voxel in $\Delta\sigma_i \in \mathbb{R}^n, (i = 1, \dots, p)$ always tends to show similar conductivity variation trend under multi-frequency scanning.

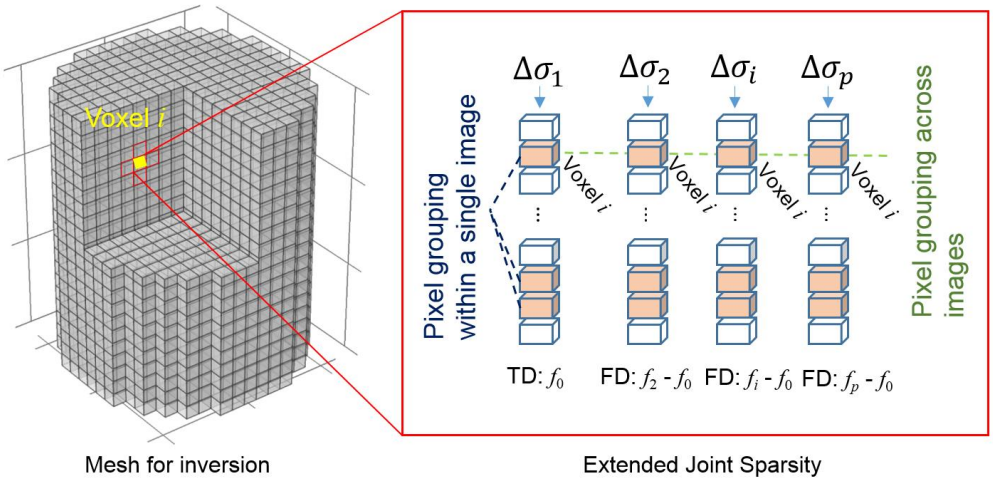

Figure 1. Schematic illustration of the idea of extended joint sparsity.

Based on the idea of extended joint sparsity, which not only considers the local structural information of an individual image but also takes into account the correlations of voxels under different frequency excitations, the mfEIT image reconstruction problem can be formulated as

$$\begin{cases} \min\limits_{Q} \ \|Q\|_{\omega,2,1} := \sum_{i=1}^{q} \omega_i \left\|Q_{S_i}\right\|_2 \\ s.t. \ \ JQ = K \end{cases} \tag{6}$$

where $\|\cdot\|_{\omega,2,1}$ denotes the weighted $l_{2,1}$ norm, which has been proved to promote group sparsity structure (Huang and Zhang, 2010). ω_i is the weight of the *i*th voxel group. S_i $(i = 1, \dots, q, q \leq n)$ denotes the set of voxel indices for the *i*th voxel group, which is calculated based on the idea of extended joint sparsity. This optimization problem can be solved by using the ADMM method following the steps given in our former work (Yang and Jia, 2017a), and its primal-based updating scheme has the following form:

$$\begin{cases} Q \leftarrow (\alpha_1 I + \alpha_2 J^T J)^{-1}(\alpha_1 Z + \alpha_2 J^T K - \mathcal{L}_1 + J^T \mathcal{L}_2) \\ Z \leftarrow \mathcal{F}\left(Q + \frac{1}{\alpha_1}\mathcal{L}_1, \frac{1}{\alpha_1}\omega\right) \\ \mathcal{L}_1 \leftarrow \mathcal{L}_1 - h_1\alpha_1(Z - Q) \\ \mathcal{L}_2 \leftarrow \mathcal{L}_2 - h_2\alpha_2(JQ - K) \end{cases} \tag{7}$$

where α_1, α_2 are penalty parameters; $Z \in \mathbb{R}^{n\times p}$ denotes the auxiliary matrix when applying ADMM; $\mathcal{L}_1, \mathcal{L}_2 \in \mathbb{R}^{n\times p}$ are multipliers. $\mathcal{F}$ represents shrinkage operator which definition can be referred to the work (Yang and Jia, 2017a). h_1, h_2 are step lengths when updating the multipliers. Based on (7), the problem depicted in (6) could be solved iteratively.

4 EXPERIMENT RESULTS AND DISCUSSION

Simultaneous impedance spectroscopic imaging experiment was conducted to verify the algorithm's performance. Figure 2(a) shows the mfEIT system and Visual Tomography 3-D imaging software used in the 3-D multi-frequency imaging experiments. Figure 2(b) presents the multi-layer EIT sensor with 16 electrodes in each layer. The inner diameter of the sensor is 287 mm and the depth of saline is 206 mm. The conductivity of saline is 0.07 $S \cdot m^{-1}$. Note that in this work, only the lower two layers of electrodes as illustrated in the figure were utilized to perform 3-D imaging.

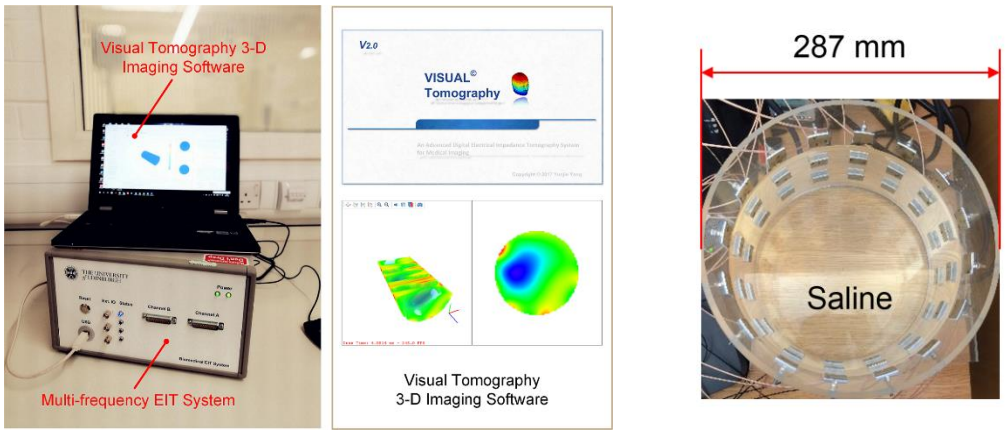

(a) (b)

Figure 2. Picture of the Edinburgh mfEIT system and Visual Tomography Software in (a) and the 3-D EIT sensor in (b).

Figure 3(a) and (b) gives the experiment phantom, where a potato was selected as sensing object since it demonstrates explicit conductivity variation over frequency. This conductivity variation is illustrated in Figure 3(c) by using Electrochemical Impedance Spectroscopy (EIS) (K'Owino and Sadik, 2005) measurement. The EIS measurement result of potato shows an increasing conductivity value over frequency.

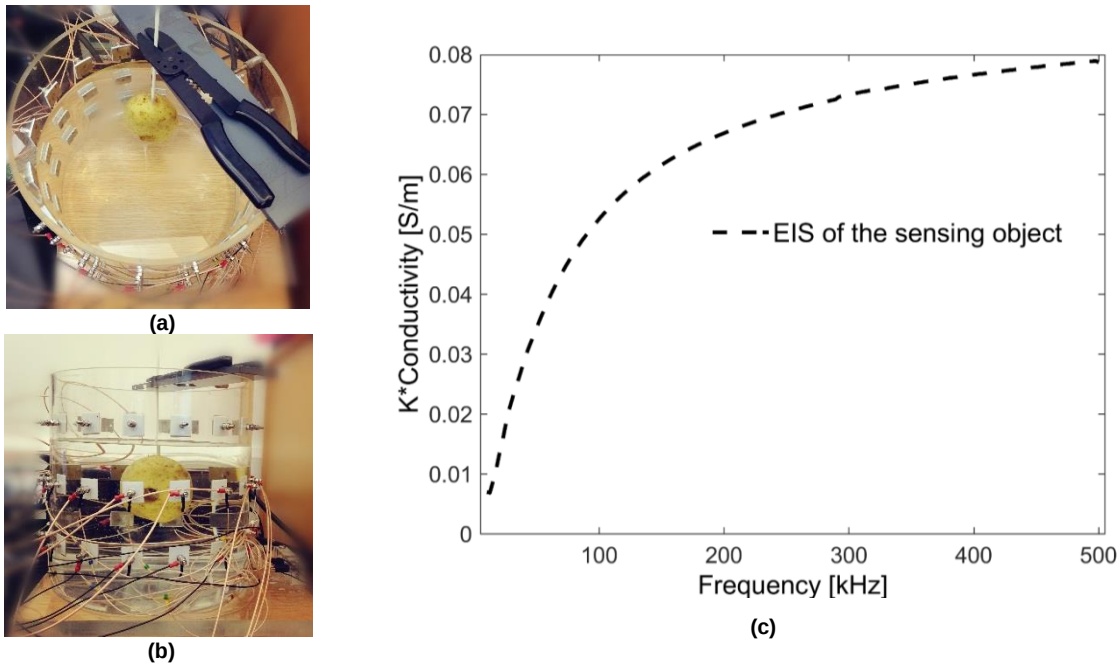

(a)

(b)

(c)

Figure 3. Experiment phantoms in top view in (a) and side view in (b) and EIS result of the potato in (c).

Three multi-frequency image reconstructions, i.e TD image reconstruction at the basic frequency 20 kHz, FD image reconstructions using 80kHz-20kHz and 40kHz-20kHz, were performed separately based on the one-step GN method firstly. The results in the format of sliced images are shown in Figure

4. Note that in these images, layer 1 corresponds to the bottom layer of the sensing region and layer 40 corresponds to the top layer of the region. In this work, the regularization parameter was set as 0.01.

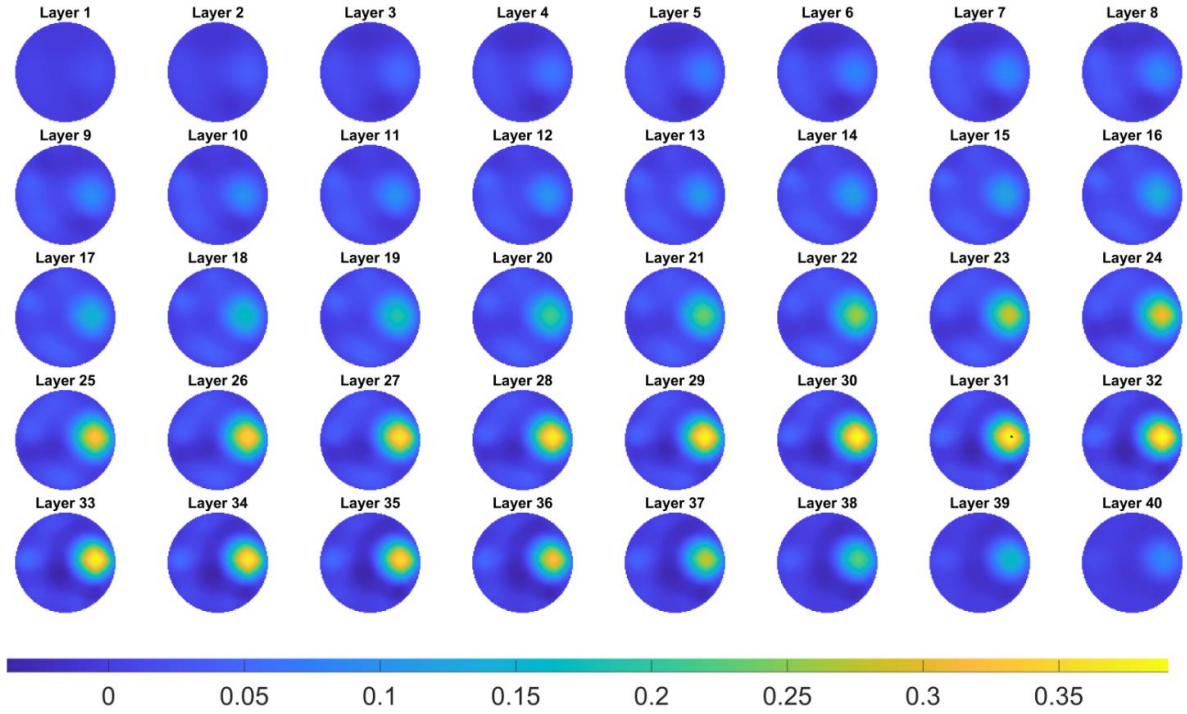

(a)

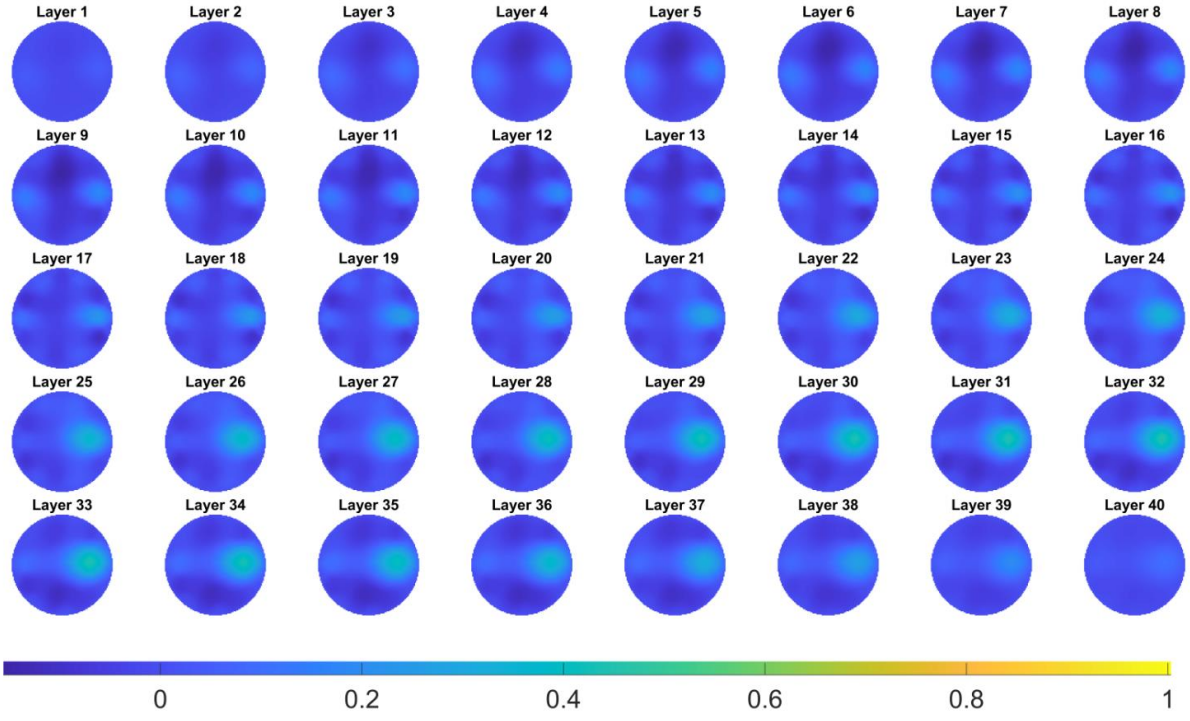

(b)

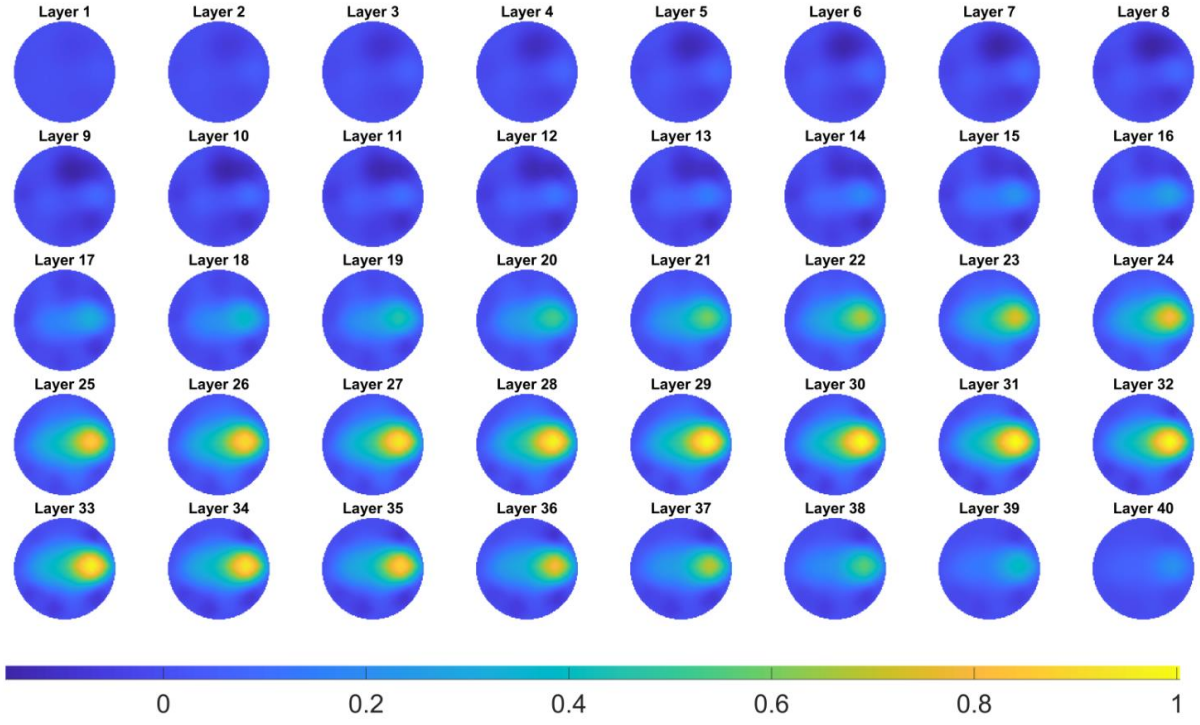

(c)

Figure 4. Multi-frequency 3-D image reconstruction results by using the one-step GN algorithm. (a) TD imaging result at 20kHz. (b) FD imaging result using 40kHz-20kHz. (c) FD imaging result using 80kHz-20kHz.

Figure 5 presents the simultaneous multi-frequency imaging results based on the proposed method. In implementing the algorithm, the maximum iteration number is set as 300 and the stopping tolerance is selected as 1e-5. The penalty parameters α_1, α_2 were set as 140 and 14, respectively. In initial guess, we assume there is no pixel grouping and problem (6) was solved first. Based on the result, the pixel grouping which is related to the structural information and frequency correlation is calculated by using the method proposed by the authors (Yang and Jia, 2017a). Thereafter, problem (6) is solved again using the updated pixel grouping results.

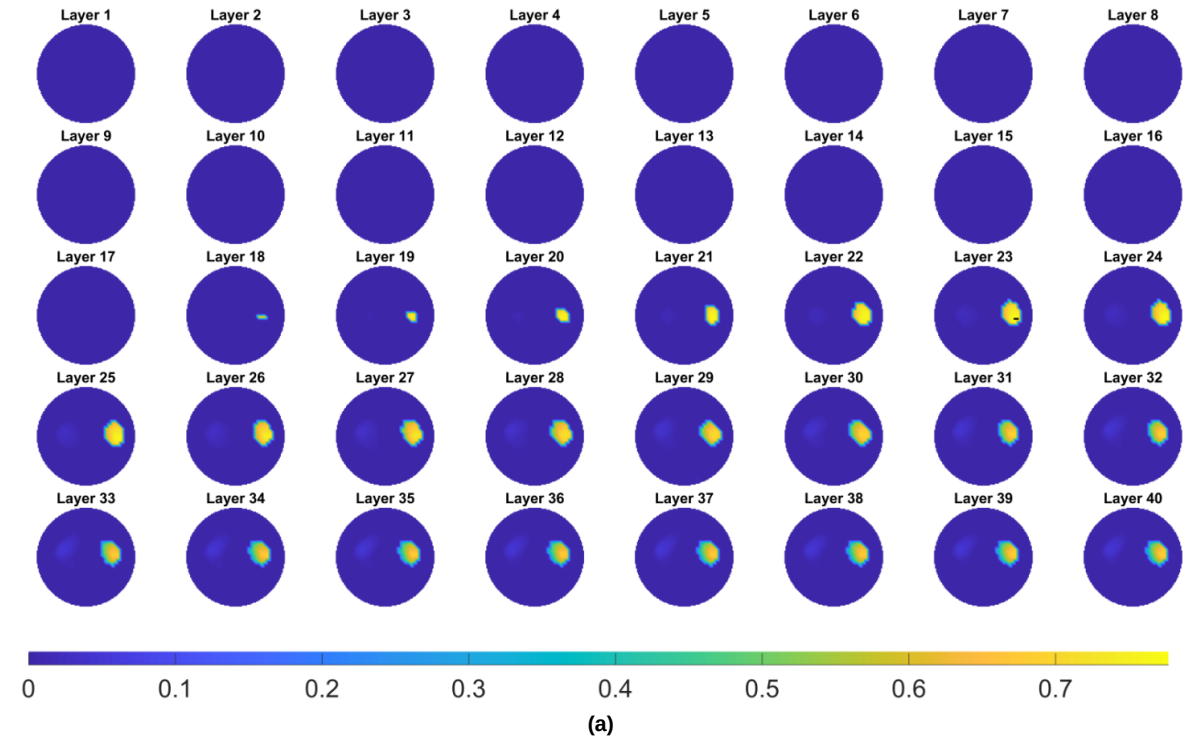

(a)

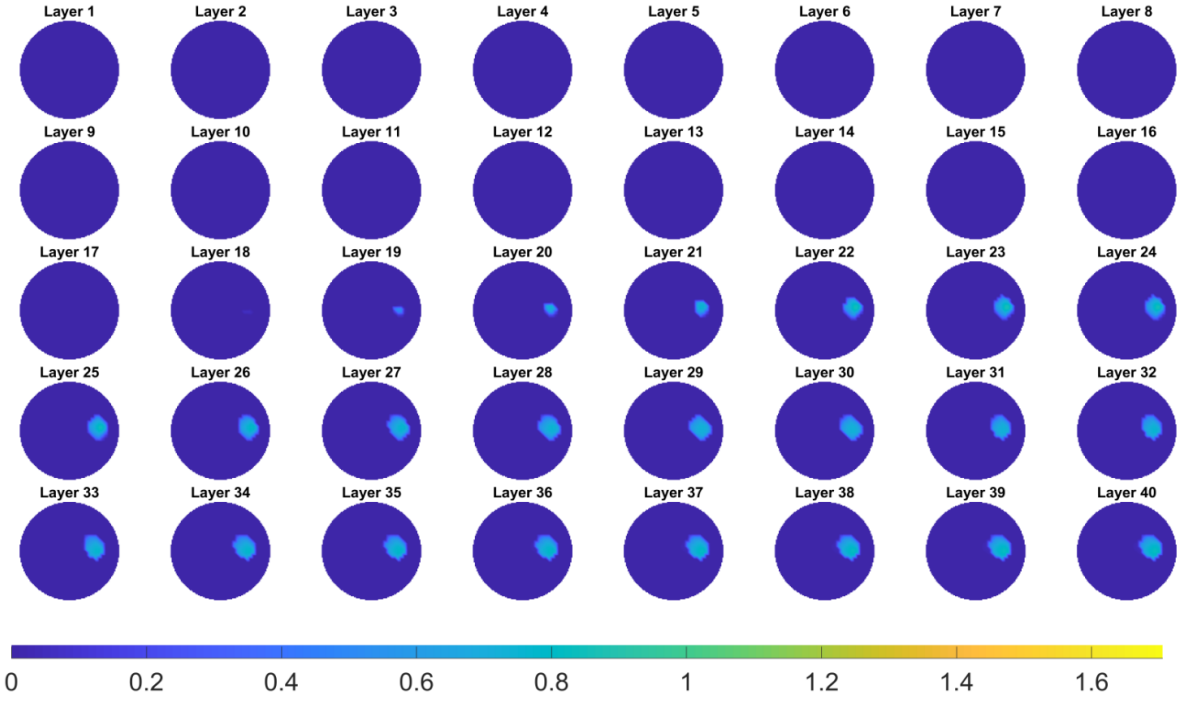

(b)

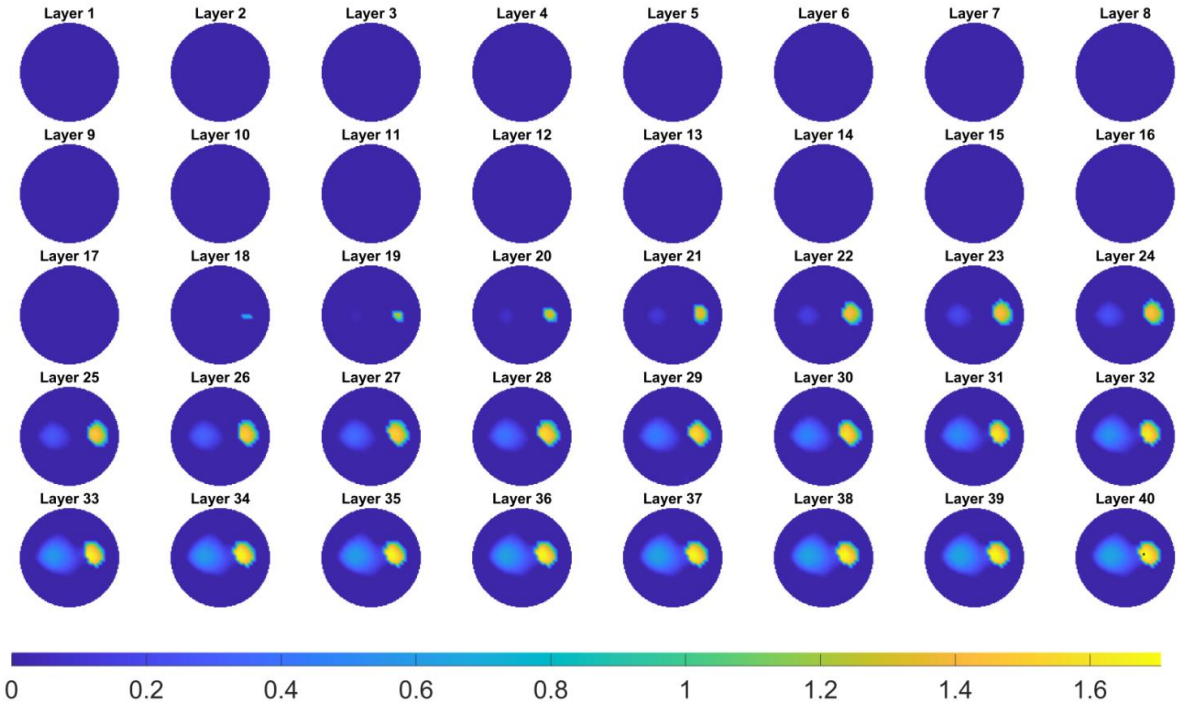

(c)

Figure 5. Multi-frequency 3-D image reconstruction results by using the proposed algorithm. (a) TD imaging result at 20kHz. (b) FD imaging result using 40kHz-20kHz. (c) FD imaging result using 80kHz-20kHz.

The experiment results demonstrated in Figure 4 and Figure 5 suggest that the proposed algorithm: a) yields higher image quality with clearer boundary and noise reduction compared with the one-step GN method; b) shows better image correlation over frequencies, which is consistent with the common knowledge and c) has the ability of simultaneous reconstructing multi-frequency 3-D images. In addition, the proposed algorithm requires lower computation cost, i.e. the elapsed time is 5.87s on a PC with

MATLAB 2017b, 24GB RAM memory and an Intel Xeon X5650 CPU. Whilst the one-step GN method takes 162.98s to calculate one image.

5 CONCLUSION

This work presents a simultaneous, fast 3-D image reconstruction algorithm for mfEIT based on extended joint sparsity. The structural prior and spatial-frequency correlations of multi-frequency 3-D image series were simultaneously exploited by extending the existing joint sparsity framework, and the resulting optimization problem was efficiently solved by employing alternating direction method of multipliers. We evaluated the performance of the method using phantom experiment, through the results of which we could confirm that the new method yields high-performance 3-D impedance spectroscopic images at a low computational cost, suggesting its great potential for future deployment in real-time 3-D impedance spectroscopic imaging applications.

REFERENCES

CHENG, K. S., ISAACSON, D., NEWELL, J. C. & GISSER, D. G. 1989. Electrode Models for Electric-Current Computed-Tomography. *IEEE Transactions on Biomedical Engineering,* 36**,** 918-924.

DONG, F., XU, Y. B., HUA, L. & WANG, H. X. 2006. Two methods for measurement of gas-liquid flows in vertical upward pipe using dual-plane ERT system. *IEEE Transactions on Instrumentation and Measurement,* 55**,** 1576-1586.

HUANG, J. Z. & ZHANG, T. 2010. The Benefit of Group Sparsity. *Annals of Statistics,* 38**,** 1978-2004.

K'OWINO, I. O. & SADIK, O. A. 2005. Impedance spectroscopy: A powerful tool for rapid biomolecular screening and cell culture monitoring. *Electroanalysis,* 17**,** 2101-2113.

LEE, B. A., KIM, B. S., KO, M. S., KIM, K. Y. & KIM, S. 2014. Electrical Resistance Imaging of Two-Phase Flow with a Mesh Grouping Technique Based on Particle Swarm Optimization. *Nuclear Engineering and Technology,* 46**,** 109-116.

MALONE, E., DOS SANTOS, G. S., HOLDER, D. & ARRIDGE, S. 2014. Multifrequency Electrical Impedance Tomography Using Spectral Constraints. *IEEE Transactions on Medical Imaging,* 33**,** 340-350.

METHERALL, P., BARBER, D. C., SMALLWOOD, R. H. & BROWN, B. H. 1996. Three-dimensional electrical impedance tomography. *Nature,* 380**,** 509-512.

POLYDORIDES, N. 2009. Linearization Error in Electrical Impedance Tomography. *Progress in Electromagnetics Research-Pier,* 93**,** 323-337.

POLYDORIDES, N. & LIONHEART, W. R. B. 2002. A Matlab toolkit for three-dimensional electrical impedance tomography: a contribution to the Electrical Impedance and Diffuse Optical Reconstruction Software project. *Measurement Science and Technology,* 13**,** 1871-1883.

SOMERSALO, E., CHENEY, M. & ISAACSON, D. 1992. Existence and Uniqueness for Electrode Models for Electric-Current Computed-Tomography. *Siam Journal on Applied Mathematics,* 52**,** 1023-1040.

WANG, M., MA, Y. X., HOLLIDAY, N., DAI, Y. F., WILLIAMS, R. A. & LUCAS, G. 2005. A high-performance EIT system. *IEEE Sensors Journal,* 5**,** 289-299.

YANG, Y., JIA, J., POLYDORIDES, N. & MCCANN, H. Effect of structured packing on EIT image reconstruction. Imaging Systems and Techniques (IST), 2014 IEEE International Conference on, 2014. IEEE, 53-58.

YANG, Y. J. & JIA, J. B. 2017a. An Image Reconstruction Algorithm for Electrical Impedance Tomography Using Adaptive Group Sparsity Constraint. *IEEE Transactions on Instrumentation and Measurement,* 66**,** 2295-2305.

YANG, Y. J. & JIA, J. B. 2017b. A multi-frequency electrical impedance tomography system for real-time 2D and 3D imaging. *Review of Scientific Instruments,* 88.

YIN, X., WU, H., JIA, J. & YANG, Y. 2018. A Micro EIT Sensor for Real-time and Non-destructive 3-D Cultivated Cell Imaging. *IEEE Sensors Journal,* 18**,** 5402-5412.